ADVANCED MATERIALS
www.advmat.de

Rapid Volumetric Bioprinting of Decellularized Extracellular Matrix Bioinks

*Liming Lian, Maobin Xie, Zeyu Luo, Zhenrui Zhang, Sushila Maharjan, Xuan Mu, Carlos Ezio Garciamendez-Mijares, Xiao Kuang, Jugal Kishore Sahoo, Guosheng Tang, Gang Li, Di Wang, Jie Guo, Federico Zertuche González, Victoria Abril Manjarrez Rivera, Ling Cai, Xuan Mei, David L. Kaplan, and Yu Shrike Zhang**

Decellularized extracellular matrix (dECM)-based hydrogels are widely applied to additive biomanufacturing strategies for relevant applications. The extracellular matrix components and growth factors of dECM play crucial roles in cell adhesion, growth, and differentiation. However, the generally poor mechanical properties and printability have remained as major limitations for dECM-based materials. In this study, heart-derived dECM (h-dECM) and meniscus-derived dECM (Ms-dECM) bioinks in their pristine, unmodified state supplemented with the photoinitiator system of tris(2,2-bipyridyl) dichlororuthenium(II) hexahydrate and sodium persulfate, demonstrate cytocompatibility with volumetric bioprinting processes. This recently developed bioprinting modality illuminates a dynamically evolving light pattern into a rotating volume of the bioink, and thus decouples the requirement of mechanical strengths of bioprinted hydrogel constructs with printability, allowing for the fabrication of sophisticated shapes and architectures with low-concentration dECM materials that set within tens of seconds. As exemplary applications, cardiac tissues are volumetrically bioprinted using the cardiomyocyte-laden h-dECM bioink showing favorable cell proliferation, expansion, spreading, biomarker expressions, and synchronized contractions; whereas the volumetrically bioprinted Ms-dECM meniscus structures embedded with human mesenchymal stem cells present appropriate chondrogenic differentiation outcomes. This study supplies expanded bioink libraries for volumetric bioprinting and broadens utilities of dECM toward tissue engineering and regenerative medicine.

1. Introduction

3D bioprinting technologies are broadly applied to building living tissue constructs for applications in regenerative engineering, including transplantation, drug screening, and disease modeling.[1-5] However, current additive biomanufacturing technologies, including but not limited to extrusion-based bioprinting,[6] stereolithographic bioprinting,[7] and digital light processing (DLP) bioprinting,[8,9] all fabricate 3D constructs in a point-by-point or layer-by-layer fashion.[8,10] This feature presents certain challenges when producing sophisticated hydrogel structures that are oftentimes mechanically weak, especially those that contain freeform architectures. In addition, for bioprinting with cell-laden bioinks, these conventional methods also are limited because of the considerable fabrication times required, which positively correlate with the sizes of the tissue constructs.[11-13] Thus, to overcome these limitations of conventional additive biomanufacturing techniques, new methodologies are needed to improve tissue bioprinting capacities.

The volumetric additive manufacturing (VAM) technology prints the entire object

L. Lian, M. Xie, Z. Luo, Z. Zhang, S. Maharjan, X. Mu, C. E. Garciamendez-Mijares, X. Kuang, G. Tang, D. Wang, J. Guo, F. Z. González, V. Abril Manjarrez Rivera, L. Cai, X. Mei, Y. S. Zhang
Division of Engineering in Medicine
Department of Medicine
Brigham and Women's Hospital
Harvard Medical School
Cambridge, MA 02139, USA
E-mail: yszhang@bwh.harvard.edu

Z. Zhang
Ragon Institute of Mass General, MIT, and Harvard
Cambridge, MA 02139, USA

J. K. Sahoo, G. Li, D. L. Kaplan
Department of Biomedical Engineering
Tufts University
Medford, MA 02155, USA

The ORCID identification number(s) for the author(s) of this article can be found under https://doi.org/10.1002/adma.202304846

DOI: 10.1002/adma.202304846

at once, thus developed to address many of the abovementioned challenges.[14] Specifically, VAM illuminates dynamically evolving light patterns into specific portions of the volume of a photoresin contained in a transparent vial, which is synergistically rotated perpendicular to the direction of incident light. As such, the photoresin is only crosslinked at desired volumes where sufficient light doses are accumulated after angular exposures with the computed planar patterns,[15] leading to solidification of the target object with optimized shape fidelity. Briefly, in contrast to conventional 3D bioprinting technologies with still slower printing speeds and sometimes insufficient surface qualities,[16] VAM can fabricate objects in a single pass with lower concentrations of bioinks, enabling much faster production rates of items, particularly those with complex geometries. These advantages of VAM on creating detailed, complicated structures make it promising for biomedical applications, such as fabricating soft tissues or organs. Although a few photoresins have been reported for VAM (or termed volumetric bioprinting when it comes to printing cell-laden bioinks),[10,17] such as silica glass,[18] acrylate polymers,[14,19] gelatin methacryloyl (GelMA),[17] gelatin-norbornene (Gel-NB),[20] and silk fibroin and sericin,[21] there remains a significant demand to develop additional bioinks to facilitate expanded applications for this new technology.

Decellularized extracellular matrices (dECM) as a class of biomaterials directly extracted from native tissues, have been widely used for tissue fabrication. dECM have similar components and compositions to their corresponding source tissues, enabling better recapitulation of intricate and cytocompatible microenvironments contributing to improved cell functionality and tissue morphogenesis than some of the conventional bioinks.[22,23] In addition, the dECM technology, after decades of advancement, can now be conveniently derived from different organs and tissues with mature protocols, leading to broadened and consistent supplies and thus expanded applications. Indeed, a number of tissues including but not limited to skin, bone, kidney, heart, cornea, liver, and vasculature,[22,24-27] have been fabricated using dECM by different additive (bio)manufacturing methods indicating the potential of this source of biomaterials.[28-32] Nevertheless, dECM bioinks are usually weak in mechanical properties and thus exhibit poor printability when used alone at low concentrations, which dramatically reduces the practicality of using dECM in the bioprinting of sophisticated tissue structures. Although some strategies such as physical supporting,[28,33,34] hybrid bioinks,[35] and chemical conjugation[36-38] were introduced to increase print fidelity and stability of dECM, limitations remain in terms of maintaining native bioactivities of pristine dECM in their unmodified state.[39]

A visible light-induced crosslinking approach was recently proposed and utilizes pristine dECM (without chemical conjugation or mixing with any other biomaterials) by taking advantage of a newer photoinitiator system, tris(2,2-bipyridyl)dichlororuthenium(II) hexahydrate/sodium persulfate (Ru/SPS).[22,40] For both extrusion-based bioprinting or DLP-based bioprinting, the dECM bioinks could be polymerized via a di-tyrosine crosslinking mechanism. Despite the success in efficient photocrosslinking during or after bioprinting, these bioprinting modalities share the same limitations as discussed above, that is, being relatively slow processes and oftentimes requiring strong mechanical properties of the bioinks for creating sophisticated volumetric tissue patterns.

In this study, we introduce the compatibility of pristine, unmodified heart-derived dECM (h-dECM) and meniscus-derived dECM (Ms-dECM) combined with Ru/SPS as a new class of bioinks for volumetric bioprinting. Generally, compared with previous 3D bioprinting strategies with dECM, our work introduces several unique aspects: i) We utilize unmodified dECMs mixed with a photoinitiator as our bioinks without needing additional biomaterial types. This approach creates microenvironments more closely resembling natural tissues than hybrid bioinks. ii) The VAM technology has allowed us to employ lower concentrations of dECMs at down to 1% compared to oftentimes the higher dECM concentrations required before, which not only conserves materials but more importantly, also exhibits superior biological compatibility. iii) Our study demonstrates the rapid fabrication speeds enabled by VAM, with the entire process taking only ≈30–45 s in most cases for both h-dECM and Ms-dECM.

To highlight the advantages of VAM, we aimed to print both hollow and solid tissue structures, with the heart representing a hollow structure and the meniscus representing a solid one. As noted, our photoinitiator system used, Ru/SPS, plays a crucial role in the process by oxidizing aromatic residues, including tyrosine. The oxidized tyrosine groups, activated by Ru/SPS, are then converted into tyrosyl free radicals, which subsequently form covalent di-tyrosine bonds with nearby tyrosine moieties.[41] Furthermore, to achieve higher crosslinking efficiency, we sought to employ dECM types with a higher content of tyrosine. In comparison to other organs, such as the brain, h-dECM, and Ms-dECM contain higher proportions of collagen, which is rich in tyrosine.[28,41] Therefore, choosing h-dECM and Ms-dECM for proof-of-concept demonstrations has allowed us to attain more rapid and better printing processes. However, the technology can be easily expanded to other dECM types in the future with further optimizations of the printing parameters. Again in general, dECM types rich in collagen, such as those from skin and lung tissues, other than the ones used here, are likely to be more readily adaptable to the VAM technology; in contrast, tissues with lower collagen contents, such as brain and kidney cortex, may pose challenges when integrating with the Ru/SPS crosslinking system without functionalization (Table S1, Supporting Information).

2. Results and Discussion

h-dECM was derived from the left ventricle of the porcine heart (**Figure 1A**; Figure S1A, Supporting Information), while Ms-dECM was obtained from the porcine meniscus (Figure 1A; Figure S1B, Supporting Information). Both types of dECM bioinks contain abundant tyrosine residue-carrying protein components that form di-tyrosine crosslinks[28,41] after photoactivation in the presence of the Ru/SPS system (Figure 1B). For exemplary demonstrations of biomedical applications of our custom-built volumetric bioprinter (Figure 1C), rat cardiac myocyte (rCM)-laden h-dECM bioinks and human induced pluripotent stem cell-derived cardiomyocyte (hiPSC-CM)-laden h-dECM bioinks, as well as human mesenchymal stem cell (hMSC)-laden Ms-dECM bioinks were prepared (Figure 1B) for bioprinting

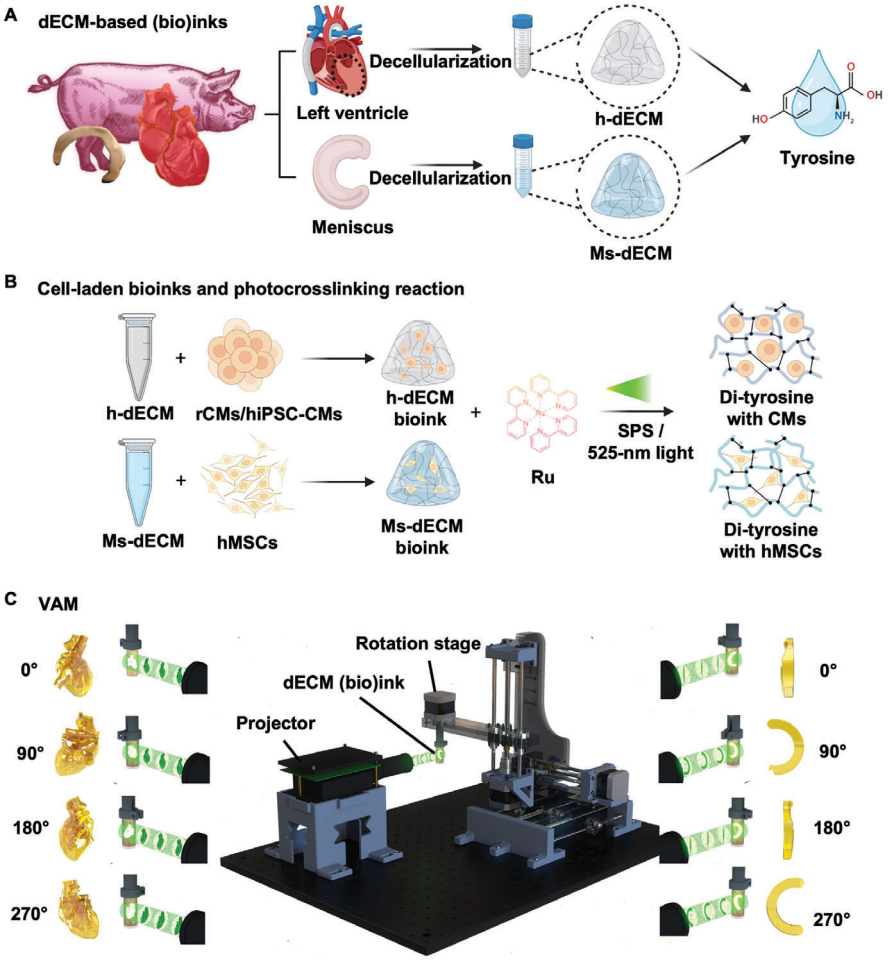

Figure 1. Schematics showing the dECM (bio)ink preparation and VAM processes. A) Decellularization of porcine heart and meniscus for obtaining h-dECM and Ms-dECM, respectively. B) Preparation of cell-laden bioinks and the photocrosslinking mechanism of dECM bioinks. C) VAM process and the customized VAM system, which mainly includes a projector, a vial-rotation motor, and a (bio)ink-containing vial. h-dECM: heart-derived decellularized extracellular matrix; Ms-dECM: meniscus-derived decellularized extracellular matrix; VAM: volumetric additive manufacturing; Ru: tris(2,2-bipyridyl)dichlororuthenium(II) hexahydrate; SPS: sodium persulfate.

of living cardiac as well as meniscus constructs, respectively (Figure 1C). The cytocompatible microenvironments of dECM along with the rapid fabrication speeds (≈45 s for h-dECM and ≈30 s for Ms-dECM) enabled by volumetric bioprinting ensured desirable functions of the embedded cells during bioprinting and post-bioprinting culture. It is believed that the volumetric bioprinting system in conjunction with light-activated dECM bioinks in their pristine, unmodified state has enormous potential for engineering hydrogel structures and tissue constructs for expanded applications in biomedicine.

For light-activated VAM with Ru/SPS, the wavelength of the projector light at 525 nm would perform better than UV-blue light.[21,42] The absorbance at 525 nm of different concentrations of h-dECM and Ms-dECM indicated that h-dECM had a higher absorbance than Ms-dECM (Figure S2A,B, Supporting Information), and dECM at high concentrations showed higher absorbance values than that at low concentrations (Figure S2C, Supporting Information). According to numerous previous studies, the ratio of Ru to SPS at 1 to 10 seems to be the best working ratio for photocrosslinking under many scenarios.[21,22,43] The mixing of dECM with varying concentrations of Ru/SPS resulted in a significant increase in absorbance values, with a gradual rise observed as the concentration of Ru/SPS was increased from 0/0 to 2/20 mM (Figure S2D, Supporting Information). The crosslinkability test was performed by photocrosslinking different formulations of h-dECM and Ms-dECM (bio)inks with 525 nm of light and 3 mW cm^{-2} of light intensity (Figure S3A,B, Supporting Information). The photocrosslinkability maps (Figure S3C, Supporting Information) clearly indicated that, i) there was insufficient material for crosslinking when the concentration of dECM was below 0.5%, and ii) the concentration of Ru/SPS below 0.25/2.5 mM could not support the photocrosslinking process of dECM at any concentration.

After printing with the photocrosslinkable formulations of the dECM (bio)inks, printability maps were further refined (**Figure 2A,B**). The 2% h-dECM (bio)ink or 1.5% Ms-dECM (bio)ink showed poor printability as they required more photoinitiator

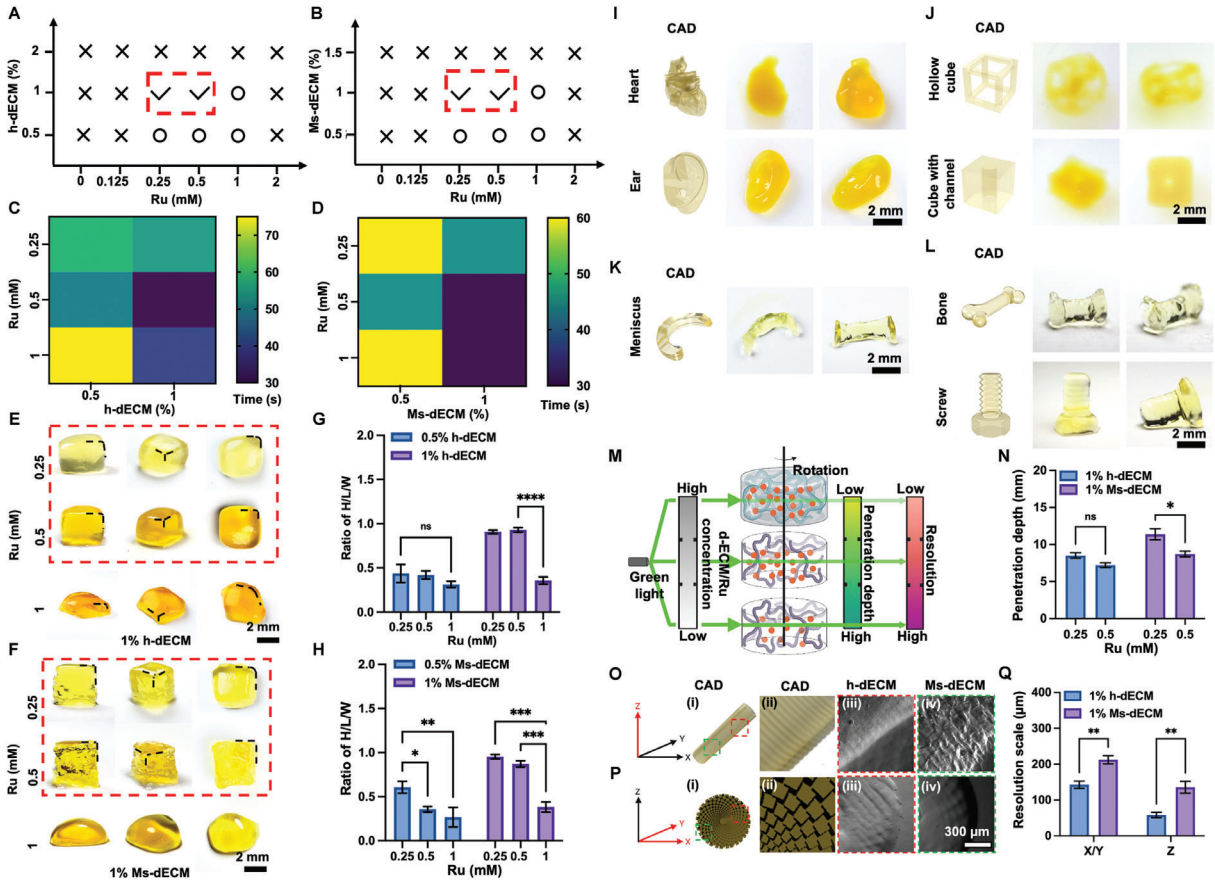

Figure 2. Printing performance of VAM with dECM (bio)inks. A,B) Printability maps of A) h-dECM (bio)ink and B) Ms-dECM (bio)ink with different formulations. √: printable; O: printable but shape not good; X: non-printable. C,D) Heat maps of printing times for 3D cubic constructs from C) h-dECM and D) Ms-dECM with different formulations. E,F) Photographs of 3D cubic construct printed using E) 1% h-dECM (bio)ink and F) 1% Ms-dECM (bio)ink with different concentrations of Ru/SPS. G,H) Quantified ratios of the height to width of the 3D cubic construct printed using G) h-dECM (bio)ink and H) Ms-dECM (bio)ink with different concentrations of Ru/SPS. I) CAD models and photographs of printed objects using 1% h-dECM with 0.5-mM Ru/5-mM SPS (light intensity: 3 mW cm^{-2}). The heart construct was printed in 45 s, and the ear construct was printed in 30 s. J) CAD models and photographs of printed objects using 1% h-dECM with 0.25-mM Ru/2.5-mM SPS (light intensity: 3 mW cm^{-2}). The cubic frame construct was printed in 60 s and the channeled cube construct was printed in 60 s. K) CAD model and photograph of printed object using 1% Ms-dECM with 0.5-mM Ru/5-mM SPS (light intensity: 3 mW cm^{-2}). The meniscus construct was printed in 30 s. L) CAD models and photographs of printed objects using 1% Ms-dECM with 0.25-mM Ru/2.5-mM SPS (light intensity: 3 mW cm^{-2}). The bone construct was printed in 45 s, and the screw structure was printed in 30 s. M) Schematic showing the effect of concentration of Ru/SPS and concentration of dECM on printing resolution. N) Quantified penetration depths of h-dECM with different formulations. O)i,ii) CAD model of the solid bar, where the thicknesses of the threads were from 1 to 101 μm. O)iii,iv) Microscopic images of the printed solid bars from 1% h-dECM (printing time: 30 s; light intensity: 3 mW cm^{-2}) and 1% Ms-dECM (printing time: 35 s; light intensity: 3 mW cm^{-2}) at 0.5-mM Ru/5-mM SPS. P)i,ii) CAD model of the radially arranged array of cubes. P)iii,iv) Microscopic images of the printed cube arrays from 1% h-dECM (printing time: 30 s; light intensity: 3 mW cm^{-2}) and 1% Ms-dECM (printing time: 35 s; light intensity: 3 mW cm^{-2}) at 0.5-mM Ru/5-mM SPS. Q) Quantified resolutions in *X*/*Y* and *Z* directions of the printed constructs. Statistical significances are expressed as $*p < 0.05$, $**p < 0.01$, $***p < 0.001$, and $****p < 0.0001$ by two-way ANOVA with Tukey's post hoc test; $n = 10$, ns = not significant. dECM: decellularized extracellular matrix; VAM: volumetric additive manufacturing; h-dECM: heart-derived decellularized extracellular matrix; Ms-dECM: meniscus-derived decellularized extracellular matrix; Ru: tris(2,2-bipyridyl)dichlororuthenium(II) hexahydrate; SPS: sodium persulfate.

to form the di-tyrosine networks, while high concentrations of Ru/SPS (over 1/10 mM) dramatically reduced the penetration depth of the incident light (Tables S2,S3, Supporting Information), which also impacted the print shape fidelity.[21,22] Of interest, 1% h-dECM and 1% Ms-dECM combined with 0.25/2.5-mM or 0.5/5-mM Ru/SPS presented better printabilities than the 0.5% h-dECM and 0.5% Ms-dECM (bio)inks. Subsequently, printing efficiencies were determined by comparing the printing times of all printable dECM (bio)ink formulations (Figure 2C,D). Remarkably, all the printing times were less than 90 s, generally faster than the traditional DLP process, which typically requires a few to tens of minutes to produce cubic constructs of the same size.[42] Furthermore, 1% h-dECM and 1% Ms-dECM with different concentrations of Ru/SPS were printed faster than 0.5% h-dECM and 0.5% Ms-dECM. To visually compare the shape fidelities of 3D constructs volumetrically printed by the different formulations of the (bio)inks, photographs of the printed cubic structures were collected (Figure 2E,F; Figure S4A,B, Supporting Information). The ratios of height to width (Figure 2G,H) and the ratios of height to length (Figure S4C,D, Supporting Information)

of the cubes were calculated to quantify the printing fidelities, confirming again that 1% h-dECM and 1% Ms-dECM mixed with 0.25/2.5-mM or 0.5/5-mM Ru/SPS had favorable printability performances than other groups.

These data suggested that the printing shape fidelity using volumetric printing heavily relied on the concentrations of the dECM and the photoinitiator system (Ru/SPS), consistent with previous reports on VAM using different (bio)ink types.[18,20,21] Compared with other conventional additive manufacturing methods such as DLP and extrusion,[22,24,44,45] the VAM process works well with significantly lower concentrations of dECM (Table S4, Supporting Information), reducing (bio)ink-preparation challenges as well as allowing lower stiffness of the constructs to be produced. Furthermore, even at a low concentration, the dECM-based bioinks naturally possessed relatively high viscosity values due to their complex macromolecular interactions, which include various extracellular matrix components.[23] This inherent viscosity behavior plays a crucial role in the VAM printing process, which generally requires thermo-reversible crosslinking or sufficient viscosities of the bioinks used. All these features are beneficial toward expanded applications of dECM biomaterials toward biomedicine.

Using the optimized formulations of dECM-based (bio)inks that showed good printing fidelities, we subsequently explored the ability to produce additional constructs with more sophisticated architectures. For example, a human heart structure containing the hollow aorta and a human ear structure (Figure 2I), as well as a Chinese temple structure and a screw structure (Figure S5A, Supporting Information), were printed with 1% h-dECM combined with 0.25/2.5-mM Ru/SPS. The heart and ear constructs were printed in ≈45 s, while the screw and the temple were printed in ≈30 s. Similarly, with 0.5/5-mM Ru/SPS, the 1% h-dECM (bio)ink was volumetrically printed into sophisticated 3D geometries, such as a cubic frame and a cube with a hollow channel (Figure 2J), both at ≈45 s. Alternatively, a human meniscus structure (≈30 s; Figure 2K) and a human ear structure (≈45 s; Figure S5B, Supporting Information) were printed using 1% Ms-dECM with 0.25/2.5-mM Ru/SPS. A human femur-like structure and a screw structure (Figure 2L) were further printed using 1% Ms-dECM containing 0.5/5-mM Ru/SPS. The good VAM performance of these optimized dECM (bio)inks illustrated the potential wide utility. Intriguingly, even for these sophisticated patterns, the printing times still only ranged from 30 to 45 s, indicating that the printing efficiency was not significantly impacted by the complexity of the structure made. Compared with the same structures such as the heart,[34] ear,[46] and screw[47] printed using other traditional additive manufacturing methods, the VAM process reduced the exposure time of the material to the external environment (from minutes/tens of minutes to tens of seconds), which would likely minimize the stress on embedded cells when cell-laden bioprinting is utilized.[10]

Due to the limitation of the penetration depth, the maximum size we could print with our dECM-VAM coupled with the Ru/SPS system was ≈10 mm for the object's diameter, substantially smaller than the actual dimensions of target organs such as the human heart or meniscus. The use of different biomaterial and photoinitiator systems (Table S5, Supporting Information) in other VAM studies had shown higher penetration depths and thus larger sizes achievable. Nevertheless, some of those materials systems, such as poly(ethylene glycol)-diacrylate would inevitably compromise cellular activities under most scenarios, bringing limitations for biomedical applications. Furthermore, it is important to note that size limitations can also vary significantly between different bioprinting technologies (Table S5, Supporting Information). Some slower but more traditional printing methods, such as DLP and extrusion, may offer the ability to produce significantly larger constructs due to their sequential point-by-point or layer-by-layer approach. However, these methods often come at the cost of increased printing time and may face challenges in achieving the same level of spatial complexities that are demonstrated with volumetric bioprinting. Additionally, those technologies impose more stringent demands on material properties, such as concentration and mechanics, which then require to apply modifications to the biomaterials or adopt hybrid biomaterial systems. Notably, with natural biomaterials such as dECM utilized in our study, other technologies so far have not demonstrated the ability generating high-fidelity structures with good complexities at low concentrations, indicating the unique advantage of the volumetric bioprinting approach adopted here despite the size limitation.

Resolution is another important parameter for volumetric bioprinting. With the known resolution (1140 × 912 pixels) of the projector, the printing resolution of the dECM-based (bio)inks was dramatically influenced by the light penetration depth, which was closely correlated with the concentrations of both dECM and Ru/SPS. The high concentration of dECM or Ru/SPS blocks light dose coming through the (bio)ink vial, which would then cause reduced penetration depth (Figure 2M). Specifically, printing using (bio)inks with poor penetration depths resulted in material crosslinking along the wall of the vial, which could change the light path and impede the crosslinking process within the central regions (Figure S6, Supporting Information). The penetration depth analyses of 525-nm light for 1% Ms-dECM (Figure 2N), for example, indicated that the Ms-(bio)ink mixed with 0.25/2.5-mM Ru/SPS exhibited a deeper penetration depth (≈12 mm), which was larger than the radius of glass vial (6 mm) used in the process; a similar situation was observed with 0.5/5-mM Ru/SPS. In comparison, all the other formulations of the (bio)ink and Ru/SPS combinations showed poor penetration depths (<6 mm; Figure S7, Supporting Information), unsuitable for VAM in our setup.

To quantify the resolutions of h-dECM and Ms-dECM, two custom-designed patterns, that is, a solid rod with bars (Figure 2Oi,ii) and a radially arranged array of cubes with different diameters (Figure 2Pi,ii) were printed using 1% h-dECM and Ms-dECM supplemented with 0.5/5-mM Ru/SPS. For the axial resolution on the vertical (*Z*) direction, the photographs of the printed solid rods (≈25 s for h-dECM and ≈30 s for Ms-dECM) showed that the size of the smallest bar thickness of the h-dECM rod was ≈79 μm, while that of Ms-dECM was ≈133 μm (Figure 2Oiii,iv), suggesting that h-dECM led to a higher printing resolution in the *Z*-axial direction than Ms-dECM under similar conditions. Furthermore, resolutions in the *X*–*Y* plane were evaluated by printing a radially arranged array of cubes with different diameters. The smallest diameter of the h-dECM cubes was ≈137 μm (Figure 2Piii), which was also better than the smallest diameter (≈207 μm) printed with Ms-dECM (Figure 2Piv). For comparison, the pattern of solid rods with bars was also printed

using h-dECM and Ms-dECM with concentrations of Ru/SPS at 0.25/2.5 mM. However, the resulting micrographs (Figure S8, Supporting Information) failed to display discernible bars, indicating a substantial reduction in printing resolution under these conditions, which warrants further investigations of improvements.

Accordingly, the results of the resolution tests (Figure 2Q) suggested that the h-dECM resulted in higher resolutions in all directions (*X*, *Y*, and *Z*) than the Ms-dECM when volumetrically printed. Since the prints were conducted under the same concentrations of Ru/SPS, such a difference in resolution could be primarily influenced by the variations in the dECM components. Molecular weight analyses by sodium dodecyl-sulfate polyacrylamide gel electrophoresis (SDS-PAGE) for h-dECM and Ms-dECM revealed the presence of three distinct bands, with the strongest band observed at ≈160 kDa and two other weaker visible bands at 260 and 35–40 kDa (Figure S9, Supporting Information), consistent with the literature.[48] Previous reports indicated that collagen is the primary component of these dECM biomaterials, while Ms-dECM also contains abundent fibronectin and thrombospondin,[49] and h-dECM has more fibronectin and elastin.[50] These different protein components and the larger cartilage fibers[51] in Ms-dECM might cause more light scattering during printing, leading to a lower resolution than for h-dECM. Overall, the printing performance and resolution were related to a combination of factors, including printing time, dECM concentration, Ru/SPS concentrations, as well as the intrinsic characteristics of the dECM, which could be inferred when expanding VAM to other (bio)inks in the future.

Mechanically, the range of compressive moduli of dECM hydrogels prepared with different crosslinking systems have been reported in the range of 0.18 to 3.0 kPa.[52,53] To evaluate the mechanical properties of dECM photocrosslinked with Ru/SPS, cylindrical constructs with a diameter at 1 cm and a thickness at 5 mm (Figure S10A, Supporting Information) were printed (30 s) with different formulations of dECM (bio)inks for compression tests (Figure S10B, Supporting Information). The moduli were measured at 10.9 ± 4.5 kPa for h-dECM printed with 0.25/2.5-mM Ru/SPS, and 28.4 ± 2.5 kPa at 0.5/5-mM Ru/SPS; for the cylinders printed using Ms-dECM, the moduli were lower than those for h-dECM constructs, at 4.1 ± 0.6 kPa for 0.25/2.5-mM Ru/SPS and 14.3 ± 1.2 kPa for 0.5/5-mM Ru/SPS (Figure S11, Supporting Information). Notably, our volumetrically printed dECM objects had higher moduli than previously reported prints of the dECM without Ru/SPS.[54] This observation could be attributed to the fact that di-tyrosine crosslinks dramatically improve the mechanical properties of dECM hydrogels compared with thermally crosslinked dECM hydrogels, up to ≈3.0 kPa.[22,55] Nevertheless, the moduli of our volumetrically printed dECM materials were still much lower than DLP-printed constructs previously reported despite the use of Ru/SPS as the photoinitiator system,[22] given the feasibility to use much smaller dECM concentrations as low as 1% in our setup.

Scanning electron microscopy (SEM) was utilized to examine the morphologies of VAM-printed dECM constructs after dehydration. Compared with the fibrous morphologies with dense and randomly oriented collagen in thermally crosslinked Ms-dECM hydrogel,[55] the cylinders volumetrically printed with Ms-dECM and Ru/SPS showed porous structures. In comparison, VAM-printed h-dECM constructs had relatively denser matrices without the presence of noticeable pores, at the same concentration of 1% used (Figure S12, Supporting Information). These results partially explained why the mechanical properties of printed h-dECM constructs were higher than those printed with Ms-dECM with the same concentrations of dECM/photoinitiator. However, it should be noted that SEM images do not necessarily reflect the actual pore sizes of the dECM constructs in their hydrated state although the trends are maintained.

The in vitro degradation profiles of the volumetrically printed 1% h-dECM and 1% Ms-dECM cylinders (with 0.25/2.5-mM Ru/SPS) were subsequently evaluated in phosphate-buffered saline (PBS), collagenase IV PBS solution, and α-chymotrypsin PBS solution at 37 °C for up to 28 days (Figure S13, Supporting Information). During the initial 2 days of the evaluations in PBS, the samples exhibited a slight swelling behavior, resulting in a ≈5% increase in their wet masses. Subsequently, the masses of the samples began to gradually decrease. Notably, the 1% h-dECM-printed samples experienced a reduction in mass to 71.5%, while the 1% Ms-dECM-printed cylinders reached a mass of 84.3% after 28 days (Figure S13A, Supporting Information), suggesting that the volumetrically printed 1% Ms-dECM samples exhibited favorable stability under physiological conditions. In contrast, all constructs degraded rapidly (in 3 h) when incubated with collagenase IV solution, since the main component of both dECM types is collagen. In the presence of α-chymotrypsin, the Ms-dECM constructs presented better stability (≈24 h) than those with h-dECM, which were digested within 12 h. These results demonstrated that the degradation profiles of VAM-printed dECM constructs were intimately related to the crosslinking densities of the prints, the dECM types, as well as the microenvironments in which they were exposed.

To evaluate cell-ladened dECM bioinks, three sophisticated structures were volumetrically bioprinted with 1×10^6 mL^{-1} of NIH/3T3 fibroblasts **Figure** 3A, an ear-like structure (45 s of bioprinting time, 1% Ms-dEM with 0.25/2.5-mM Ru/SPS), a heart-like structure (45 s of bioprinting time, 1% h-dECM with 0.25/2.5-mM Ru/SPS), and a screw structure (30 s of bioprinting time, 1% Ms-dECM with 0.5/5-mM Ru/SPS). These structures were generated with good shape fidelity (Figure 3B) indicating that the printing performance was not significantly influenced by the encapsulated cells within the dECM.

Viabilities of the fibroblasts encapsulated in different formulations of dECM bioinks were assessed by live/dead assay for up to 14 days of culture (Figure 3C,D; Figure S15A,B, Supporting Information), indicating that cells embedded in all bioink formulations evaluated remained viable. However, the viabilities of cells embedded in both 1% h-dECM and 1% Ms-dECM bioprinted with 0.25/2.5-mM Ru/SPS were higher than those for the cells in dECM bioprinted with 0.5/5-mM Ru/SPS (Figure S16A,B, Supporting Information), likely due to the reduced phototoxcity when a lower concentration of photoinitiator was used. Additionally, the cell proliferation rates and metabolic activities within both 1% h-dECM and 1% Ms-dECM with 0.25/2.5-mM Ru/SPS increased over 14 days, while the metabolic activities of cells with 0.5/5-mM Ru/SPS reminded steady in the late stage, suggesting that the cells stopped proliferating or reduced their metabolic activities after 7 days (Figure 3E,F).

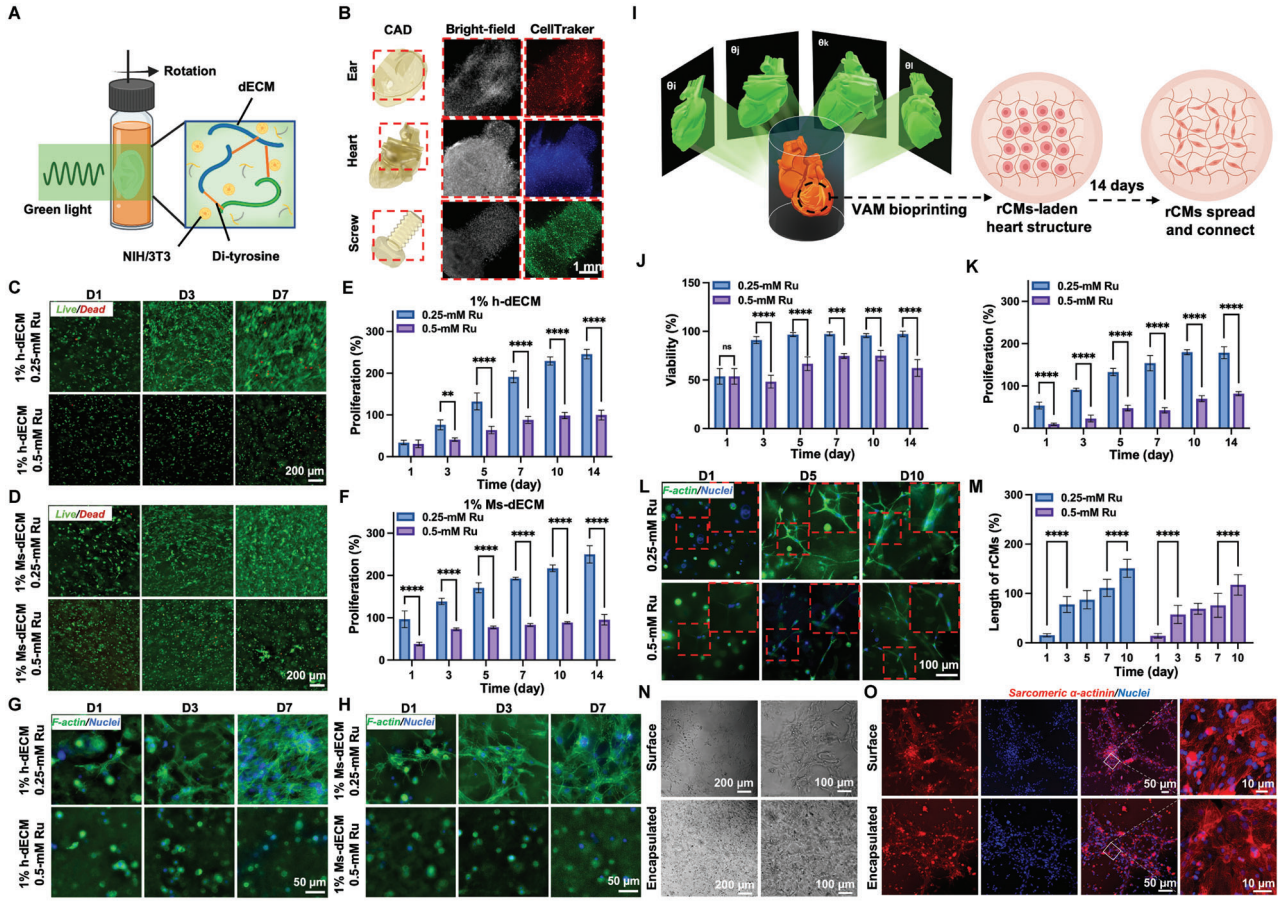

Figure 3. Cytocompatibility of dECM bioinks and characterizations of cardiac tissues volumetrically bioprinted using the rCM- or hiPSC-CM-laden h-dECM bioink. A) Schematic showing the process of volumetric bioprinting with cell-laden d-ECM bioinks. B) CAD models and microscopic images of the structures volumetrically bioprinted with NIH/3T3 fibroblast-laden dECM bioinks. The ear structure was bioprinted with 1% Ms-dECM and 0.25/2.5-mM Ru/SPS in 30 s (cells were stained with red CellTracker). The heart structure was bioprinted with 1% h-dECM and 0.25/2.5-mM Ru/SPS in 45 s (cells were stained with blue CellTracker). The screw structure was bioprinted with 1% Ms-dECM and 0.25/2.5-mM Ru/SPS in 30 s (cells was stained with green CellTracker). C,D) Micrographs showing live/dead staining of NIH/3T3 fibroblasts bioprinted within C) 1% h-dECM constructs and D) 1% Ms-dECM constructs at different concentrations of Ru/SPS for 7 days. E,F) Metabolic activity profiles of NIH/3T3 fibroblast bioprinted within E) 1% h-dECM constructs and F) 1% Ms-dECM constructs at different concentrations of Ru/SPS for 7 days. G, H) F-actin staining micrographs of NIH/3T3 fibroblasts grown within bioprinted G) 1% h-dECM and H) 1% Ms-dECM constructs at different concentrations of Ru/SPS for 7 days. I) Schematic showing the volumetric bioprinting process of heart-like structure and the process of rCM spreading. J,K) J) Quantified cell viability values and K) metabolic activity profiles of rCMs grown in the heart-like constructs bioprinted using 1% h-dECM at different concentrations of Ru/SPS for 14 days. L,M) L) Micrographs of F-actin staining and M) quantified lengths of rCM spread in the heart-like constructs bioprinted using 1% h-dECM at different concentrations of Ru/SPS for 14 days. N,O) Micrographs showing N) brightfield and O) fluorescent immunostaining of hiPSC-CMs both on the surface and encapsulated in the heart-like constructs bioprinted using 1% h-dECM and 0.25/2.5-mM Ru/SPS reaching a stretching morphology and expressing sarcomeric-α-actinin after culturing for 10 days. Statistical significances are expressed as $*p < 0.05$, $**p < 0.01$, $***p < 0.001$, and $****p < 0.0001$ by two-way ANOVA with Tukey's post hoc test. In Figures (D,F,K, and L), $n = 3$; in Figures (H,J, and N), $n = 10$; ns = not significant. dECM: decellularized extracellular matrix; VAM: volumetric additive manufacturing; Ru: ruthenium (II) hexahydrate; SPS: sodium persulfate; h-dECM: heart-derived decellularized extracellular matrix; Ms-dECM: meniscus-derived decellularized extracellular matrix; Ru: tris(2,2-bipyridyl)dichlororuthenium(II) hexahydrate; SPS: sodium persulfate; rCMs: rat cardiac myocytes; hiPSC-CMs: human induced pluripotent stem cell-derived cardiomyocytes.

Similarly, when examining the morphologies of the cells, the embedded fibroblasts only spread in the 1% h-dECM and 1% Ms-dECM volumetrically bioprinted with 0.25/2.5-mM Ru/SPS, cultured for up to 14 days (Figure 3G, H; Figure S17A,B, Supporting Information). Specifically, the size of the cells in the dECM constructs produced in the presence of 0.5/5-mM Ru/SPS did not significantly change over the culture period (15.06 ± 1.63 μm), whereas the length of the cells in dECM bioprinted with 0.25/2.5-mM Ru/SPS increased in the first 7 days (up to 85.12 ± 13.17 μm) and remained stable thereafter (Figure S18, Supporting Information). The overall favorable cytocompatibility of dECM as exhibited in these results was consistent with previous reports suggesting low crosslinking densities for light-activated bioprinting are well-suited for culturing cells of soft tissue-origin.[56-58]

Furthermore, Ru/SPS is generally considered to be less cytotoxic than some other photoinitiators.[40,43] However, its potential cytotoxicity can still affect the cytocompatibility of bioprinted

dECM constructs when cells are exposed to high concentrations of Ru/SPS for longer periods. Compared with the 1/10-mM[43] and 2/20-mM[22] Ru/SPS used in some previous studies, the 0.25/2.5-mM or 0.5/5-mM Ru/SPS adopted in most of our work is significant lower, potentially leading to a reduced cytotoxic effect. In addition, we conducted further analyses on the Ru/SPS-release from the volumetrically printed structures. Photographs clearly illustrated color changes in the samples when they were immersed in PBS at 37 °C over a 24-h period (Figure S19A, Supporting Information). By measuring the optical absorbance values of the buffer, we determined that Ru/SPS was released ≈55.3% from h-dECM and 49.4% from Ms-dECM within the first 30 min after printing, and eventually reaching to a ≈100% release for h-dECM and ≈94% for Ms-dECM (Figure S19B, Supporting Information). Accordingly, the Ru/SPS photoinitiator used in our approach at low concentrations and was rapidly released from the constructs may bring advantages for future biomedical applications.

Finally, to demonstrate that tissue-specific constructs could be fabricated via volumetric bioprinting of dECM bioinks, a human heart-like structure was created using rCM-laden h-dECM bioink containing different concentrations of Ru/SPS (0.25/2.5 mM and 0.5/5 mM; Figure 3I). The viability of rMCs was evaluated using the live/dead assay (Figure S20, Supporting Information). It was observed that the rCMs encapsulated in the cardiac tissue constructs volumetrically bioprinted with 0.25/2.5-mM Ru/SPS remained >95% viable even after 14 days of culture; in contrast, the bioprinted constructs with 0.5/5-mM Ru/SPS only showed ≈50–75% viability for the cells during the same culture period (Figure 3J). The cellular metabolic activities of rCMs encapsulated in the cardiac constructs bioprinted with 0.25/2.5-mM Ru/SPS were also significantly higher than cells in the other group (Figure 3K). These cellular results on rCMs aligned well with those on NIH/3T3 fibroblasts, confirming that our h-dECM bioink formulations might be generally suitable for soft tissue engineering using volumetric bioprinting.

Moreover, *F*-actin staining indicated that over 95% rCMs spread in the cardiac structures volumetrically bioprinted with 0.25/2.5-mM Ru/SPS after 7 days of culture, while the cells still only partially (30–40%) spread in those bioprinted with 0.5/5-mM Ru/SPS during the same culture period (Figure 3L,M; Figure S21, Supporting Information), different from the observations with fibroblasts where no cells spread in the denser matrices. As h-dECM readily captures the matrix components that are found in the native cardiac tissue, such as relevant proteins, glycosaminoglycans, and proteoglycans,[59] it could provide cells derived from the same tissue source with an appropriate microenvironment to support cell viability and spreading.

To further demonstrate the functions of the bioprinted heart-like constructs with h-dECM, samples were prepared using 1% h-dECM and 0.25/2.5-mM Ru/SPS, integrated with the human iPSC-derived cardiomyocytes (hiPSC-CMs). The brightfield microscopic images (Figure 3N) revealed the morphologies of hiPSC-CMs, showing cellular spreading both on the surfaces and within the matrix following a 10-day culturing period. Notably, the spontaneous beating movements of hiPSC-CMs were observed for cells in both configurations as well, from day 5 of bioprinting. Videos S1 and S2 (Supporting Information) respectively show the synchronized contractions of hiPSC-CMs recorded on day 10 for cells on the surface and encapsulated within the matrix of the bioprinted samples. Similarly, the immunofluorescence staining of hiPSC-CMs for sarcomeric-α-actinin on both seeded and encapsulated samples on day 10 demonstrated the development of sarcomere structures, indicating the structural maturation of hiPSC-CMs under both conditions (Figure 3O). Sarcomeric-α-actinin is the key protein in the structure and function of cardiomyocytes and plays a crucial role in the organization of the contractile apparatus in muscle cells, particularly in the sarcomere.[60] As such, this cardiac model not only offers a novel platform for the study of heart-related diseases but also holds potential as a strategic approach in cardiac tissue engineering and transplantation applications in the future.

A step further in illustrating the potential of different types of dECM used toward biomedical applications, meniscus constructs laden with hMSCs were also volumetrically bioprinted using 1% Ms-dECM containing 0.25/2.5-mM or 0.5/5-mM Ru/SPS. hMSCs sustained high viability values at ≈95% across 14 days of culture (**Figure** 4A,B), validating the favorable cytocompatibility of Ms-dECM with the cells. Similar to the results obtained from the other cell types, the cellular metabolic activities of hMSCs encapsulated in the meniscus constructs bioprinted with 0.25/2.5-mM Ru/SPS were almost twice as high as the cells in the denser constructs, by 14 days (Figure 4C). Interestingly, extensive spreading (≈100%) of hMSCs was observed in both meniscus constructs irrespective of the crosslinking density (Figure 4D; Figure S22, Supporting Information), again suggesting tissue-specificity of the dECM bioinks in directing cellular behavior matching the origins of the biomaterial.

We subsequently evaluated the functional performance of the meniscus tissues volumetrically bioprinted using 1% Ms-dECM in combination with 0.25/2.5-mM Ru/SPS. The constructs were transferred to and cultured in a chondrogenic differentiation medium for 3 weeks after 2 weeks of initial culture in proliferation medium. *F*-actin staining of the differentiated chondrocytes further indicated that the cells not only expanded in cell lengths but also in widths (Figure 4E), consistent with previous reports.[28,55] Immunostaining of the menisci showed that the expression of collagen and aggrecan improved in the 3-week period (Figure 4F), validating successful differentiation of hMSCs into the chondrocyte lineage. The expression of chondrogenesis-related genes obtained by quantitative polymerase chain reaction (qPCR), including aggrecan (*ACAN*), cartilage oligomeric matrix protein (*COMP*), collagen type I alpha 1 chain (*COL1α1*), elastin (*ELN*), and type X collagen (*COL10A1*) (Figure 4G), also validated the immunostaining results. Specifically, the expressions of COL10A1 and ELN increased significantly during the 3 weeks, while the expression of COL1A1 also increased post-differentiation, although not to a statistically significant degree. In an image revealing the morphology of the entire meniscus structure at 5 weeks of culture (Figure 4H), the embedded, expanded, and differentiated hMSCs were evident (Figure S23, Supporting Information), and the shape of the meniscus did not change, indicating the stability of the cell-laden VAM-bioprinted tissue-like constructs.

Finally, to demonstrate the general morphology and the production of glycosaminoglycans (GAGs) of the hMSCs during chondrogenic differentiation in the bioprinted tissues, the samples were histologically stained with hematoxylin and eosin

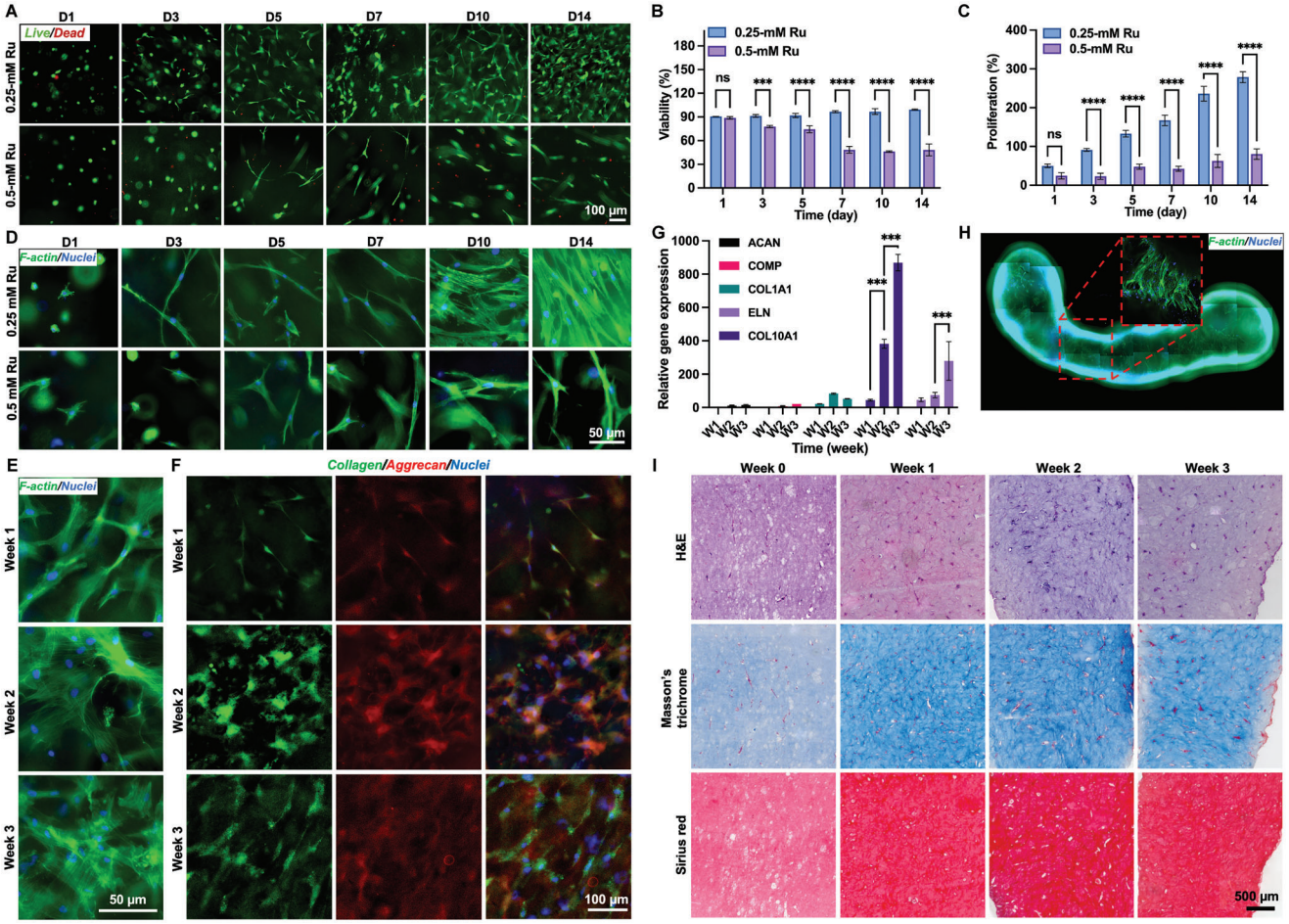

Figure 4. Characterizations of meniscus tissues volumetrically bioprinted using the hMSC-ladened Ms-dECM bioink. A–C) A) Micrographs of live/dead staining, as well as quantified B) cell viability values and C) proliferation profiles of hMSCs grown in the meniscus constructs bioprinted using 1% Ms-dECM at different concentrations of Ru/SPS. D) Micrographs showing *F*-actin staining of hMSCs spread in the bioprinted meniscus constructs. E) Micrographs showing F-actin staining of hMSCs in the meniscus constructs bioprinted using 1% Ms-dECM and 0.25/2.5-mM Ru/SPS over 3 weeks of differentiation. F) Micrographs showing immunostaining of hMSCs in the meniscus constructs bioprinted using 1% Ms-dECM and 0.25/2.5-mM Ru/SPS expressing different levels of collagen and aggrecan over 3 weeks of differentiation. G) Quantified expression levels of representative genes indicating chondrogenic differentiation status in 3 weeks. H) Low-magnification micrograph showing *F*-actin staining of hMSC-ladened meniscus tissue printed using 1% Ms-dECM and 0.25/2.5-mM Ru/SPS at 3 weeks of differentiation. The inset shows a confocal image of the high-density differentiated chondrocytes. I) Histology images of H&E, Masson's trichrome, and Sirius red staining for the bioprinted meniscus constructs printed using 1% Ms-dECM and 0.25/2.5-mM Ru/SPS containing hMSCs after 3 weeks of chondrogenic differentiation. Statistical significances are expressed as $*p < 0.05$, $**p < 0.01$, $***p < 0.001$, and $****p < 0.0001$ by two-way ANOVA with Tukey's post hoc test; $n = 3$, ns = not significant. dECM: decellularized extracellular matrix; Ru: tris(2,2-bipyridyl)dichlororuthenium(II) hexahydrate; SPS: sodium persulfate. hMSCs: human mesenchymal stem cells; Ms-dECM: meniscus-derived decellularized extracellular matrix.

(H&E), Masson's trichrome, and Sirius red (Figure 4I). Compared with the undifferentiated samples (week 0), H&E-staining images revealed the presence of typical triangular and ovoid-shaped chondrocytes,[61] which filled the normal-appearing lacunae of the constructs over time. Masson's trichrome and Sirius red staining revealed that the cartilage extracellular matrix components, including collagen and GAGs,[62,63] were present in the volumetrically bioprinted meniscus structures during the entire course of culture. However, the staining became more intense with time of differentiation, which suggested that chondrogenic differentiation successfully induced the additional secretion of cartilage-relevant ECM components. Since the limited vascularization in the native meniscus leads to poor self-regenerative capability, this VAM bioprinted meniscus provides a potential strategy for related biomedical applications for meniscus transplantation,[49] among other applications.

Our VAM-dECM system has indeed realized partial functionality in the bioprinted structures, such as the synchronized beating of hiPSC-CMs within h-dECM and the differentiation of hMSCs in Ms-dECM. Nonetheless, there are still substantial differences between these and native tissues in terms of structure, biology, and mechanics.[64] Native tissues consist of a complex array of cells, extracellular matrix, and signaling molecules, all arranged in specific architectures optimal for their functions,[65] whereas dECM is created by the decellularization process, which alters the ultrastructure potentially deviating from the tissue's

native mechanical properties and biological functionality to various extents.[25] Besides, native tissues possess inherent biological signals and dynamic environments that support cell behaviors and tissue regeneration. dECM retains many of the signaling cues and growth factors from the original tissue, but the processing of decellularization may lead to a reduction or alteration of these components, which can influence cellular responses such as migration and differentiation.[25] For example, due to the decellularization process changing the structural features such as molecular arrangements, fiber alignments, and possible loss or denaturation of extracellular matrix proteins, a critical disparity is observed in the mechanical properties. The compressive modulus of native heart tissue ranges from 30–60 kPa[66] and that of the meniscus from 600–1000 kPa,[67] whereas our bioprinted cardiac and meniscal structures approximated only 10 kPa each. All these differences, nevertheless, have provoked us with some directions for future works: i) Including a multi-material bioprinting system to emulate more structurally relevant tissue structures with multiple tissue interfaces.[68] ii) Incorporating various cell types to establish a more realistic microenvironment, promoting extensive cell–cell interactions and diverse signaling pathways. iii) Integrating dECM with other biocompatible materials to enhance mechanical properties or cell-responsiveness without compromising the bioactivities of the dECM.[69,70]

3. Conclusion

The potential for time-effective fabrication of hydrogel-based tissue constructs by VAM was demonstrated, using natural and unmodified dECM (bio)inks. With optimized formulations, both h-dECM and Ms-dECM showed significant print fidelity for sophisticated structures. Of interest, compared with the conventional layer-by-layer additive biomanufacturing methods, volumetric bioprinting was able to work with low-concentrations of dECM at a fast fabrication speed. Based on the favorable cytocompatibility of h-dECM and Ms-dECM, two proof-of-concept demonstrations of volumetrically bioprinted cardiac and meniscus constructs were illustrated. The spreading and contraction behaviors of rCMs and hiPSC-CMs encapsulated in the h-dECM heart-like constructs, as well as appropriate chondrogenic differentiation and gene expression of hMSCs embedded in the Ms-dECM meniscus constructs, were demonstrated. In conclusion, this work explored a key biomaterial, that is, dECM as (bio)inks for VAM, expanding the bioink library for this technology, while simultaneously broadening the applications of dECM-based biomaterials in biomedicine.

Supporting Information

Supporting Information is available from the Wiley Online Library or from the author.

Acknowledgements

L.L., M.X., Z.L., and Z.Z. contributed equally to this work. This work was performed in part at the Center for Nanoscale Systems (CNS), Harvard University, and supported by the National Institutes of Health (P41EB027062, R01AR070975, R01EB028143, R01HL165176, R01HL166522, R01CA282451, R21EB030257), the National Science Foundation award (1541959, CBET-EBMS-1936105, CISE-IIS-2225698), the ARO (W911NF2120130), the AFOSR (FA9550-20-1-0363), the Chan Zuckerberg Initiative (2022-316712), and the Brigham Research Institute.

Conflict of Interest

Y.S.Z. consulted for Allevi by 3D Systems, sits on the scientific advisory board and holds options of Xellar, neither of which, however, participated in or biased the work.

Data Availability Statement

The data that support the findings of this study are available from the corresponding author upon reasonable request.

Keywords

bioprinting, decellularized extracellular matrices (dECMs), tissue engineering, vat-polymerization, visible light, volumetric additive manufacturing

Received: May 22, 2023
Revised: December 28, 2023
Published online:

[1] S. V. Murphy, A. Atala, *Nat. Biotechnol.* **2014**, *32*, 773.
[2] L. Lian, C. Zhou, G. Tang, M. Xie, Z. Wang, Z. Luo, J. Japo, D. Wang, J. Zhou, M. Wang, W. Li, S. Maharjan, M. Ruelas, J. Guo, X. Wu, Y. S. Zhang, *Adv. Healthcare Mater.* **2022**, *11*, 2102411.
[3] D. Wang, S. Maharjan, X. Kuang, Z. Wang, L. S. Mille, M. Tao, P. Yu, X. Cao, L. Lian, L. Lv, J. J. He, G. Tang, H. Yuk, C. K. Ozaki, X. Zhao, Y. S. Zhang, *Sci. Adv.* **2022**, *8*, eabq6900.
[4] A. J. Vargas, C. C. Harris, *Nat. Rev. Cancer* **2016**, *16*, 525.
[5] M. A. Heinrich, W. Liu, A. Jimenez, J. Yang, A. Akpek, X. Liu, Q. Pi, X. Mu, N. Hu, R. M. Schiffelers, J. Prakash, J. Xie, Y. S. Zhang, *Small* **2019**, *15*, 1805510.
[6] W. Liu, Z. Zhong, N. Hu, Y. Zhou, L. Maggio, A. K. Miri, A. Fragasso, X. Jin, A. Khademhosseini, Y. S. Zhang, *Biofabrication* **2018**, *10*, 024102.
[7] X. Li, B. Liu, B. Pei, J. Chen, D. Zhou, J. Peng, X. Zhang, W. Jia, T. Xu, *Chem. Rev.* **2020**, *120*, 10793.
[8] J. Liao, C. Ye, J. Guo, C. E. Garciamendez-Mijares, P. Agrawal, X. Kuang, J. O. Japo, Z. Wang, X. Mu, W. Li, T. Ching, L. S. Mille, C. Zhu, X. Zhang, Z. Gu, Y. S. Zhang, *Mater. Today* **2022**, *56*, 29.
[9] S. You, J. Guan, J. Alido, H. H. Hwang, R. Yu, L. Kwe, H. Su, S. Chen, *J. Manuf. Sci. Eng.* **2020**, *142*, 081002.
[10] P. N. Bernal, P. Delrot, D. Loterie, Y. Li, J. Malda, C. Moser, R. Levato, *Adv. Mater.* **2019**, *31*, 1904209.
[11] M. de Ruijter, A. Ribeiro, I. Dokter, M. Castilho, J. Malda, *Adv. Healthcare Mater.* **2019**, *8*, 1800418.
[12] L. Moroni, T. Boland, J. A. Burdick, C. De Maria, B. Derby, G. Forgacs, J. Groll, Q. Li, J. Malda, V. A. Mironov, C. Mota, M. Nakamura, W. Shu, S. Takeuchi, T. B. F. Woodfield, T. Xu, J. J. Yoo, G. Vozzi, *Trends Biotechnol.* **2018**, *36*, 384.
[13] M. Müller, E. Öztürk, Ø. Arlov, P. Gatenholm, M. Zenobi-Wong, *Ann. Biomed. Eng.* **2017**, *45*, 210.
[14] B. E. Kelly, I. Bhattacharya, H. Heidari, M. Shusteff, C. M. Spadaccini, H. K. Taylor, *Science* **2019**, *363*, 1075.
[15] D. Loterie, P. Delrot, C. Moser, *Nat. Commun.* **2020**, *11*, 852.

[16] S. Jing, L. Lian, Y. Hou, Z. Li, Z. Zheng, G. Li, G. Tang, G. Xie, M. Xie, *Biofabrication* **2023**, *16*, 012004
[17] P. N. Bernal, M. Bouwmeester, J. Madrid-Wolff, M. Falandt, S. Florczak, N. G. Rodriguez, Y. Li, G. Größbacher, R.-A. Samsom, M. van Wolferen, L. J. W. van der Laan, P. Delrot, D. Loterie, J. Malda, C. Moser, B. Spee, R. Levato, *Adv. Mater.* **2022**, *34*, 2110054.
[18] J. T. Toombs, M. Luitz, C. C. Cook, S. Jenne, C. C. Li, B. E. Rapp, F. Kotz-Helmer, H. K. Taylor, *Science* **2022**, *376*, 308.
[19] H. Tetsuka, S. R. Shin, *J. Mater. Chem. B* **2020**, *8*, 2930.
[20] R. Rizzo, D. Ruetsche, H. Liu, M. Zenobi-Wong, *Adv. Mater.* **2021**, *33*, 2102900.
[21] M. Xie, L. Lian, X. Mu, Z. Luo, C. E. Garciamendez-Mijares, Z. Zhang, A. López, J. Manríquez, X. Kuang, J. Wu, J. K. Sahoo, F. Z. González, G. Li, G. Tang, S. Maharjan, J. Guo, D. L. Kaplan, Y. S. Zhang, *Nat. Commun.* **2023**, *14*, 210.
[22] H. Kim, B. Kang, X. Cui, S.-H. Lee, K. Lee, D.-W. Cho, W. Hwang, T. B. F. Woodfield, K. S. Lim, J. Jang, *Adv. Funct. Mater.* **2021**, *31*, 2011252.
[23] M. T. Wolf, K. A. Daly, E. P. Brennan-Pierce, S. A. Johnson, C. A. Carruthers, A. D'Amore, S. P. Nagarkar, S. S. Velankar, S. F. Badylak, *Biomaterials* **2012**, *33*, 7028.
[24] Q. Mao, Y. Wang, Y. Li, S. Juengpanich, W. Li, M. Chen, J. Yin, J. Fu, X. Cai, *Mater. Sci. Eng., C* **2020**, *109*, 110625.
[25] X. Zhang, X. Chen, H. Hong, R. Hu, J. Liu, C. Liu, *Bioact. Mater.* **2022**, *10*, 15.
[26] J. P. Zambon, I. K. Ko, M. Abolbashari, J. Huling, C. Clouse, T. H. Kim, C. Smith, A. Atala, J. J. Yoo, *Acta Biomater.* **2018**, *75*, 226.
[27] F. Potere, B. Belgio, G. A. Croci, S. Tabano, P. Petrini, G. Dubini, F. Boschetti, S. Mantero, *Front. Bioeng. Biotechnol.* **2022**, *10*, 918690.
[28] F. Pati, J. Jang, D.-H. Ha, S. W. Kim, J.-W. Rhie, J.-H. Shim, D.-H. Kim, D.-W. Cho, *Nat. Commun.* **2014**, *5*, 3935.
[29] G. Gao, J. H. Lee, J. Jang, D. H. Lee, J.-S. Kong, B. S. Kim, Y.-J. Choi, W. B. Jang, Y. J. Hong, S.-M. Kwon, D.-W. Cho, *Adv. Funct. Mater.* **2017**, *27*, 1700798.
[30] J. Kim, I. K. Shim, D. G. Hwang, Y. N. Lee, M. Kim, H. Kim, S.-W. Kim, S. Lee, S. C. Kim, D.-W. Cho, J. Jang, *J. Mater. Chem. B* **2019**, *7*, 1773.
[31] W. Han, N. K. Singh, J. J. Kim, H. Kim, B. S. Kim, J. Y. Park, J. Jang, D.-W. Cho, *Biomaterials* **2019**, *224*, 119496.
[32] J. Jang, H.-J. Park, S.-W. Kim, H. Kim, J. Y. Park, S. J. Na, H. J. Kim, M. N. Park, S. H. Choi, S. H. Park, S. W. Kim, S.-M. Kwon, P.-J. Kim, D.-W. Cho, *Biomaterials* **2017**, *112*, 264.
[33] D. B. Kolesky, K. A. Homan, M. A. Skylar-Scott, J. A. Lewis, *Proc. Natl. Acad. Sci. U. S. A.* **2016**, *113*, 3179.
[34] A. Lee, A. R. Hudson, D. J. Shiwarski, J. W. Tashman, T. J. Hinton, S. Yerneni, J. M. Bliley, P. G. Campbell, A. W. Feinberg, *Science* **2019**, *365*, 482.
[35] C. Yu, X. Ma, W. Zhu, P. Wang, K. L. Miller, J. Stupin, A. Koroleva-Maharajh, A. Hairabedian, S. Chen, *Biomaterials* **2019**, *194*, 1.
[36] D. B. Kolesky, R. L. Truby, A. S. Gladman, T. A. Busbee, K. A. Homan, J. A. Lewis, *Adv. Mater.* **2014**, *26*, 3124.
[37] G. Gao, J. Y. Park, B. S. Kim, J. Jang, D.-W. Cho, *Adv. Healthcare Mater.* **2018**, *7*, 1801102.
[38] W. Kim, C. H. Jang, G. H. Kim, *Nano Lett.* **2019**, *19*, 8612.
[39] M. Gonen-Wadmany, R. Goldshmid, D. Seliktar, *Biomaterials* **2011**, *32*, 6025.
[40] K. S. Lim, B. S. Schon, N. V. Mekhileri, G. C. J. Brown, C. M. Chia, S. Prabakar, G. J. Hooper, T. B. F. Woodfield, *ACS Biomater. Sci. Eng.* **2016**, *2*, 1752.
[41] B. Bathish, M. Paumann-Page, L. N. Paton, A. J. Kettle, C. C. Winterbourn, *J. Biol. Chem.* **2020**, *295*, 12697.
[42] M. Wang, W. Li, J. Hao, A. Gonzales, Z. Zhao, R. S. Flores, X. Kuang, X. Mu, T. Ching, G. Tang, Z. Luo, C. E. Garciamendez-Mijares, J. K. Sahoo, M. F. Wells, G. Niu, P. Agrawal, A. Quiñones-Hinojosa, K. Eggan, Y. S. Zhang, *Nat. Commun.* **2022**, *13*, 3317.
[43] K. S. Lim, B. J. Klotz, G. C. J. Lindberg, F. P. W. Melchels, G. J. Hooper, J. Malda, D. Gawlitta, T. B. F. Woodfield, *Macromol. Biosci.* **2019**, *19*, 1900098.
[44] A. Abaci, M. Guvendiren, *Adv. Healthcare Mater.* **2020**, *9*, 2000734.
[45] X. Ma, C. Yu, P. Wang, W. Xu, X. Wan, C. S. E. Lai, J. Liu, A. Koroleva-Maharajh, S. Chen, *Biomaterials* **2018**, *185*, 310.
[46] W. Li, M. Wang, L. S. Mille, J. A. Robledo Lara, V. Huerta, T. Uribe Velázquez, F. Cheng, H. Li, J. Gong, T. Ching, C. A. Murphy, A. Lesha, S. Hassan, T. B. F. Woodfield, K. S. Lim, Y. S. Zhang, *Adv. Mater.* **2021**, *33*, 2102153.
[47] G. S. Perrone, G. G. Leisk, T. J. Lo, J. E. Moreau, D. S. Haas, B. J. Papenburg, E. B. Golden, B. P. Partlow, S. E. Fox, A. M. S. Ibrahim, S. J. Lin, D. L. Kaplan, *Nat. Commun.* **2014**, *5*, 3385.
[48] A. R. Pereira, A. Lipphaus, M. Ergin, S. Salehi, D. Gehweiler, M. Rudert, J. Hansmann, M. Herrmann, *Materials* **2021**, *14*, 4431.
[49] E. A. Makris, P. Hadidi, K. A. Athanasiou, *Biomaterials* **2011**, *32*, 7411.
[50] T. T. Aye, A. Scholten, N. Taouatas, A. Varro, T. A. B. Van Veen, M. A. Vos, A. J. R. Heck, *Mol. BioSyst.* **2010**, *6*, 1917.
[51] A. J. S. Fox, A. Bedi, S. A. Rodeo, *Sports Health* **2012**, *4*, 340.
[52] J. Jang, T. G. Kim, B. S. Kim, S.-W. Kim, S.-M. Kwon, D.-W. Cho, *Acta Biomater.* **2016**, *33*, 88.
[53] G. Ahn, K.-H. Min, C. Kim, J.-S. Lee, D. Kang, J.-Y. Won, D.-W. Cho, J.-Y. Kim, S. Jin, W.-S. Yun, J.-H. Shim, *Sci. Rep.* **2017**, *7*, 8624.
[54] B. D. Elder, S. V. Eleswarapu, K. A. Athanasiou, *Biomaterials* **2009**, *30*, 3749.
[55] J. Wu, Q. Ding, A. Dutta, Y. Wang, Y.-h. Huang, H. Weng, L. Tang, Y. Hong, *Acta Biomater.* **2015**, *16*, 49.
[56] M. Xie, D. Fan, Y. Li, X. He, X. Chen, Y. Chen, J. Zhu, G. Xu, X. Wu, P. Lan, *Int. J. Nanomed.* **2017**, *12*, 7751.
[57] V. Fitzpatrick, Z. Martin-Moldes, A. Deck, R. Torres-Sanchez, A. Valat, D. Cairns, C. Li, D. L. Kaplan, *Biomaterials* **2021**, *276*, 120995.
[58] C. Qi, J. Liu, Y. Jin, L. Xu, G. Wang, Z. Wang, L. Wang, *Biomaterials* **2018**, *163*, 89.
[59] D. Bejleri, M. E. Davis, *Adv. Healthcare Mater.* **2019**, *8*, e1801217.
[60] N. Silbernagel, A. Körner, J. Balitzki, M. Jaggy, S. Bertels, B. Richter, M. Hippler, A. Hellwig, M. Hecker, M. Bastmeyer, N. D. Ullrich, *Biomaterials* **2020**, *227*, 119551.
[61] A. Karim, A. K. Amin, A. C. Hall, *Kaibogaku Zasshi* **2018**, *232*, 686.
[62] D. O. Visscher, H. Lee, P. P. M. van Zuijlen, M. N. Helder, A. Atala, J. J. Yoo, S. J. Lee, *Acta Biomater.* **2021**, *121*, 193.
[63] S. Chae, S.-S. Lee, Y.-J. Choi, D. H. Hong, G. Gao, J. H. Wang, D.-W. Cho, *Biomaterials* **2021**, *267*, 120466.
[64] E. S. Mameri, S. P. Dasari, L. M. Fortier, F. G. Verdejo, S. Gursoy, A. B. Yanke, J. Chahla, *Curr. Rev. Musculoskeletal Med.* **2022**, *15*, 323.
[65] B. N. Brown, S. F. Badylak, *Transl. Res.* **2014**, *163*, 268.
[66] S. Baghersad, A. Sathish Kumar, M. J. Kipper, K. Popat, Z. Wang, *J. Funct. Biomater.* **2023**, *14*, 269.
[67] A. Morejon, C. D. Norberg, M. De Rosa, T. M. Best, A. R. Jackson, F. Travascio, *Front. Bioeng. Biotechnol.* **2021**, *8*, 622552.
[68] S. Chae, U. Yong, W. Park, Y.-m. Choi, I.-H. Jeon, H. Kang, J. Jang, H. S. Choi, D.-W. Cho, *Bioact. Mater.* **2023**, *19*, 611.
[69] X. Cui, J. Li, Y. Hartanto, M. Durham, J. Tang, H. Zhang, G. Hooper, K. Lim, T. Woodfield, *Adv. Healthcare Mater.* **2020**, *9*, 1901648.
[70] H. W. Ooi, S. Hafeez, C. A. van Blitterswijk, L. Moroni, M. B. Baker, *Mater. Horiz.* **2017**, *4*, 1020.